Received: 1 November 2021 | Revised: 19 January 2022 | Accepted: 11 February 2022

DOI: 10.1002/mp.15568

RESEARCH ARTICLE

MEDICAL PHYSICS

Toward 3D dose verification of an electronic brachytherapy source with a plastic scintillation detector

Peter Georgi[1] | **Gustavo Kertzscher**[2] | **Lars Nyvang**[2] | **Jaroslav Šolc**[3] | **Thorsten Schneider**[4] | **Kari Tanderup**[1,2] | **Jacob Graversen Johansen**[1,2]

[1]Department of Clinical Medicine, Aarhus University, Aarhus, Denmark

[2]Department of Oncology, Aarhus University Hospital, Aarhus N, Denmark

[3]Photon Dosimetry Laboratory, Czech Metrology Institute, Prague, Czech Republic

[4]Division for Ionizing Radiation, WG 6.34 "Dosimetry for Brachytherapy and Beta Radiation Protection", Physicalisch-Technische Bundesanstalt (PTB), Braunschweig, Germany

Correspondence
Peter Georgi, Department of Clinical Medicine, Aarhus University, Palle Juul-Jensens Boulevard 82, DK-8200 Aarhus N, Denmark.
Email: pegeor@clin.au.dk

Funding information
EMPIR from Participating States and from the European Union's Horizon 2020 research and innovation Programme, Grant/Award Number: 18NRM02 PRISM-eBT; Novo Nordisk Fonden, Grant/Award Number: NNF19OC0058756

Abstract

Background: Electronic brachytherapy (eBT) is considered a safe treatment with good outcomes. However, eBT lacks standardized and independent dose verification, which could impede future use.

Purpose: To validate the 3D dose-to-water distribution of an electronic brachytherapy (eBT) source using a small-volume plastic scintillation detector (PSD).

Methods: The relative dose distribution of a Papillon 50 (P50) (Ariane Medical Systems, UK) eBT source was measured in water with a PSD consisting of a cylindrical scintillating BCF-12 fiber (length: 0.5 mm, Ø: 1 mm) coupled to a photodetector via an optical fiber. The measurements were performed with the PSD mounted on a motorized stage in a water phantom (MP3) (PTW, Germany). This allowed the sensitive volume of the PSD to be moved to predetermined positions relative to the P50 applicator, which pointed vertically downward while just breaching the water surface. The percentage depth-dose (PDD) was measured from 0 to 50 mm source-to-detector distance (SDD) in 1–3 mm steps. Dose profiles were measured along two perpendicular axes at five different SDDs with step sizes down to 0.5 mm. Characterization of the PSD consisted of determining the energy correction through Monte Carlo (MC) simulation and by measuring the stability and dose rate linearity using a well-type ionization chamber as a reference. The measured PDD and profiles were validated with corresponding MC simulations.

Results: The measured and simulated PDD curves agreed within 2% (except at 0 mm and 43 mm depth) after the PSD measurements were corrected for energy dependency. The absorbed dose decreased by a factor of 2 at 7 mm depth and by a factor of 10 at 26 mm depth. The measured dose profiles showed dose gradients at the profile edges of more than 50%/mm at 5 mm depth and 15%/mm at 50 mm depth. The measured profile widths increased 0.66 mm per 1 mm depth, while the simulated profile widths increased 0.74 mm per 1 mm depth. An azimuthal dependency of $> 10\%$ was observed in the dose at 10 mm distance from the beam center. The total uncertainty of the measured relative dose is $< 2.5\%$ with a positional uncertainty of 0.4 mm. The measurements for a full 3D dose characterization (PDD and profiles) can be carried out within 8 h, the limiting factor being cooling of the P50.

Conclusion: The PSD and MP3 water phantoms provided a method to independently verify the relative 3D dose distribution in water of an eBT source.

KEYWORDS
dose verification, electronic brachytherapy, Monte Carlo dosimetry, plastic scintillators

1 | INTRODUCTION

Electronic brachytherapy (eBT) is a radiotherapy modality that utilizes low-energy X-rays (< 100 keV) for contact X-ray therapy (CXRT) or intraoperative radiotherapy (IORT). EBT is considered a safe treatment with good clinical outcomes. However, reports have shown occurrences of unacceptable levels of dose misadministration that could harm patients.[1] This is partially due to nearly nonexistent independent dose verification, despite existing guidelines for kilovoltage dosimetry.[2] Instead, dose prescriptions are solely based on vendor-supplied dose maps. A probable reason is the lack of affordable equipment and feasible methods that can be implemented in the clinical workflow without excessively increasing the workload. Additionally, the variety of eBT systems is extensive. Thus, dosimetry methods should optimally be transferable across these systems. The absence of independent dose verification could impede the future use of eBT. Therefore, dose-verification quality assurance (QA) has been suggested to be performed annually and following repair or service of eBT sources.[3] Standardized QA should, as a minimum, provide the clinical staff with a tool to deliver dose to malignant tissue with uncertainties of less than ±5%, as recommended by the American Association of Physicists in Medicine (AAPM).[2,4]

The verification of a clinical source's dose distribution in water serves as an essential QA procedure. Such procedures are rarely carried out in clinics and are not standardized for eBT sources. Therefore, reliable in-water dose verification methods should be developed and thoroughly verified. The steep dose gradients (> 10%/mm close to the source) associated with eBT lead to a high demand on the spatial resolution of the dose measurements.[3,5] Thus, a small-volume dosimeter whose position can be precisely controlled and monitored is needed. Ionization chambers and radiochromic films are typical dosimeters investigated in eBT-related literature.[1,3,5–9] Although they provide reliable dose-rate readings, ionization chambers are subject to a large number of correction factors. Radiochromic films, on the other hand, offer no temporal resolution of the output of the radiation source, and variation in dose rate is thus not registered. Plastic scintillation detector (PSD) systems are promising candidates for eBT dose verification. They can be made in submillimeter dimensions and can provide time-resolved measurements.

PSDs consist of a small piece of scintillating plastic coupled to a photodetector via an optical fiber. When exposed to radiation, the scintillating plastic responds by emitting light. Multiple plastic scintillators show excellent dose–response linearity and emission consistency for therapeutic photon energies > 100 keV.[10–12] However, a known source of undesired light production is luminescence in the irradiated optic fiber.[13] This luminescence contributes to the light reaching the photodetector. Different methods have proven effective in removing this so-called *stem signal*.[13–19] Cherenkov radiation is a large component of the stem signal addressed by these methods but is only produced by Compton electrons with energies above 180 keV.[14] Photon energies are typically < 100 keV in eBT, where fluorescence is therefore the main contributor. However, the stem-removal methods are still effective. Another concern is the non-water equivalence of PSDs. They are almost water equivalent in terms of interaction with high-energy photons (> 125 keV),[20] but this is not the scenario for eBT. The absorption efficiency of a PSD relative to water decreases with decreasing photon energy.[21–23] Additionally, substantial quenching occurs due to low-energy secondary electrons with high linear energy transfer. Water nonequivalence and quenching therefore pose a challenge for accurate dosimetry demanding material- and radiation-specific corrections. With detailed knowledge of the beam quality and photon spectrum, these factors can be obtained with appropriate Monte Carlo (MC) simulations.[21,23] Accounting for this, a sufficiently small PSD could prove feasible for measuring the steep dose gradients of eBT. That is, if it can be precisely positioned relative to the source.

A way to ensure accurate positioning would be through the usage of commercially available water phantoms with a motorized stage. They offer full scatter conditions and allow for the accurate placement of small dosimeters. Some phantoms can position the in-build stage with 0.1 mm precision.[1]

The purpose of this work was to prove that the dose distribution of an eBT source can be independently verified with a PSD system. It is part of the PRISM-eBT project (Primary standards and traceable measurement methods for X-ray emitting electronic brachytherapy devices) with the overall goal of carrying out prenormative research on eBT to simplify and harmonize eBT dosimetry procedures and provide metrological input to standardization bodies.[24]

The investigation was based on the Papillon 50 (P50) eBT source (Ariane Medical Systems, UK). Its dose distribution was measured with a laboratory-developed PSD system in a high-precision motorized MP3 water phantom (PTW, Germany). The PSD system was

[1] Data sheet for the MP3 water phantom (PTW): https://www.ptwdosimetry.com/en/products/mp3-water-phantom-system/.

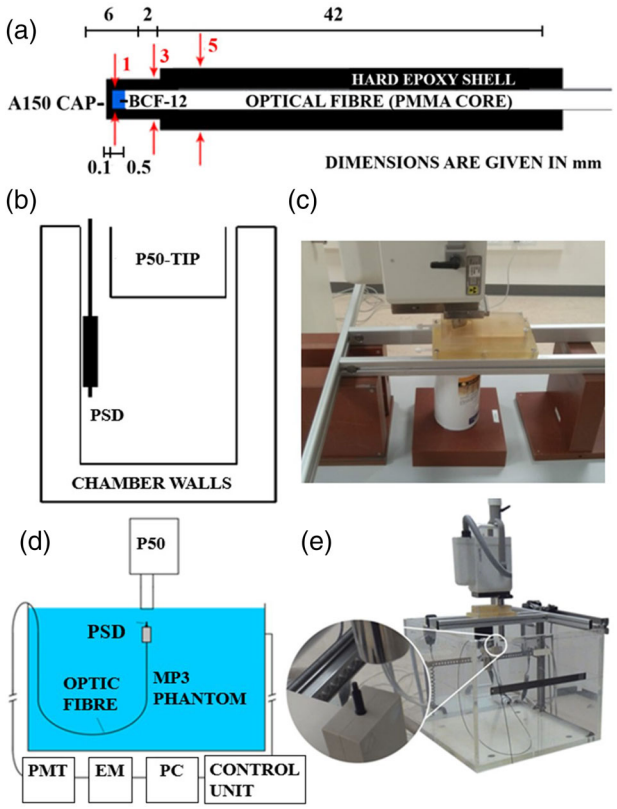

FIGURE 1 (a) Sketch of the dosimeter probe. (b) Sketch and (c) picture of the setup used for dosimeter and source stability measurements. (d) Sketch and (e) picture of the experimental setup used for 3D dose distribution measurements

thoroughly characterized under P50 irradiation conditions. Energy corrections were obtained with the Geant4 MC code wrapper, TOPAS.[25,26] MC simulation was also used to validate the measured dose distribution.

2 | MATERIALS AND METHODS

2.1 | Materials

The dose distribution of a P50 source was measured in a water phantom using a PSD. The main components are shown in Figure 1d–e. The measured dose distribution was validated against results obtained from MC simulations. The individual measurement components and MC tools are described in this section. In addition, equipment used to characterize the stability of the PSD system, the P50 output, and system specific correction factors are described.

2.1.1 | The source

P50 is a focus-to-spot-distance (FSD) source that delivers photons via a 50 kVp X-ray tube (Figure 1c and e). Its composition has been described in detail in the literature.[3,27] Electrons are accelerated in a copper tube and hit a thin rhenium target, generating bremsstrahlung. Characteristic X-rays are removed through a thin beryllium and carbon filter, and the beam is flattened with a series of aluminum plates. The X-ray tube is encapsulated in a stainless-steel rod with a 21 mm outer diameter. Cylindrical steel applicators can be placed over the rod, effectively shaping the beam and varying the delivered surface dose rate. For this study, an applicator with a 25 mm inner diameter was used.

2.1.2 | Detectors

The PSD was developed at Physicalisch-Technische Bundesanstalt (PTB, Braunschweig Germany) (Figure 1a). The sensitive probe consisted of a cylindrical scintillating polystyrene fiber (BCF-12) (Saint-Gobain, France) 0.5 mm in length and 1 mm in diameter. The scintillator was coupled to a photomultiplier tube (PMT) (H5783 SEL2, Hamamatsu) via a fiber-optic cable and encapsulated in a thin hard epoxy shell to protect it from damage and light leaks. The optical fiber consisted of a 1 mm diameter PMMA core, with 10 μm fluorinated polymer cladding, and a 0.5 mm polyethylene jacket. The numerical aperture of the fiber was 0.5. The PMT transforms the light signal from the scintillator into a charge. An electrometer (Unidos Webline, PTW) recorded the accumulated charge over a given time to determine the average dose rate. Only relative measurements were performed; hence, no calibration from charge to absolute dose was performed. An almost identical probe, with the scintillating volume replaced by bare optical fiber (BF probe) made from PMMA, was used to account for stem-signal, Section 2.2.3.

A well-type ionization chamber (WTCh) (HDR1000PLUS, Standard Imaging) was used as a reference detector for experiments characterizing the PSD system and P50 output. The WTCh signal was measured with an electrometer (CDX2000B, Standard Imaging).

2.1.3 | The phantom

The dose-distribution measurements were all performed in an MP3 water phantom (PTW, Germany). It consisted of a large plexiglass tank ($600 \times 500 \times 408$ mm^3) placed on top of a pumping system allowing for quick filling and emptying of water. The phantom had an inbuilt motorized stage that allowed for accurate placement of the detector in all three dimensions. The dedicated holders were designed in-house to provide stable positioning of the P50 and the PSD. Using the software Mephysto (PTW, Germany), the stage was moved to preprogrammed

dwell positions with custom dwell times. Both the coordinate of each dwell position and the corresponding PSD signal as read by the electrometer were recorded and stored in a single text file by Mephysto.

2.1.4 | Monte Carlo simulation of energy dependence and dose distribution

MC simulation was used to determine the energy dependence of the PSD. This simulation utilized a measured spectrum of the P50 to define the source output.

The measured dose distribution was validated against a second MC simulation including the accelerated electrons and full process of producing bremsstrahlung and filtering.

All simulations were performed on an Intel Xeon Gold 6154 3 GHz 16-core CPU using the Geant4 wrapper TOPAS.[25,26]

2.2 | Methods

The experiments can be divided into three subsections. First, a characterization of the measurement components was performed. The PSD system's response when exposed to the very low-energetic photons of P50 was characterized. Characterization included signal stability, dose-rate linearity, and energy dependence. The temporal output stability of P50 was characterized simultaneously. The positional uncertainty of the motorized phantom stage was analyzed as well. Second, the actual dose-distribution measurements were performed. Third, the measured dose distribution was validated against MC simulation. The methods are described in the following section.

2.2.1 | Source stability and detector dose–response linearity

The stability of the PSD signal was measured by simultaneously exposing it and the WTCh to a series of identical P50 irradiations in a static setup and comparing the signals. The PSD was taped to the inner wall of the WTCh with the sensitive tip two-thirds of the WTCh height from its WTCh opening (Figure 1b–c). The P50 X-ray tube, encapsulated by the 25 mm inner diameter applicator, was placed one-third down the WTCh. This position was purely chosen due to the available space in the WTCh. Since the proper signal was received in both detectors, this was deemed appropriate. The detectors were irradiated continuously for 300 seconds while measuring the detector signals over 10 second intervals. The irradiation was repeated six times. A decrease in the P50 output dose rate was observed, and a time factor, T(t), was defined as the ratio between the mean dose rate and the instantaneous dose rate. This factor was used to correct for temporal changes in output dose-rate for the later dose-distribution measurements.

The linearity between the detector response and dose rate was investigated by using the same setup but varying the current in the P50 X-ray tube to values between 0.3 mA and 3.0 mA in steps of 0.1–0.2 mA. Six irradiations of 60 s were performed for currents 0.3 to 1.0 mA and four for currents 1.2 to 3.0 mA. The current values were randomly ordered. These measurements were used to determine a linearity factor, $L(\dot{S}_{PSD})$, accounting for any nonlinearity between the dose rate, $\dot{D}_W(r)$, at position r and detector response, $\dot{S}_{PSD}$. $L(\dot{S}_{PSD})$ was defined as the ratio between the WTCh signal and the PSD signal $\dot{S}_{PSD}$ when normalized to the mean PSD response at a 1.5 mA P50 current. The standard deviation (SD) of the discrepancy between the relative PSD and WTCh signals was used as an estimate of the PSD intrinsic uncertainty at different dose rates.

PSD energy dependence

The energy dependence of the PSD was determined with MC simulation. The simulation was performed using a disc source placed in the center of the top surface of a $600 \times 600 \times 600$ mm^3 cubic water phantom. The source diameter was 20 mm and emitted photons with a uniform angular spread of 45^o into the phantom. The emission spectrum was defined according to a measured P50 spectrum (Figure 4). The spectrum was measured in air 25 cm away from P50 with an Amptek X-123 CdTe X-ray spectrometer using a set of three tungsten collimators placed one after another with 50 μm, 100 μm, and 200 μm nominal aperture diameters. In the simulation, 1 mm^3 cubic scoring volumes were placed at distances of 0 to 50 mm in 5 mm steps along an axis perpendicular to the source disc intersecting its center. For the first simulation, the scoring volumes were defined as water, while they were defined as polystyrene for the second. Simulation was run until 1 SD of the scored dose was below 3%. The energy dependence of the PSD was defined as the ratio between the simulated dose to water and polystyrene, $E(r) = D_W(r)/D_{poly}(r)$, having normalized the doses at 10 mm depth. Physical parameters and material properties were defined according to the Penelope physics list[28] and Geant4 material list.[29(p4)]

Precision of MP3 phantom stage positioning

The precision of the MP3 phantom stage positioning was investigated with a camera (HDR-CX260VE, Sony) by filming the stage traveling along three axes. The filmed positions were compared with those recorded by Mephysto. The camera was placed 2.5 m from the phantom walls to make perspective effects negligible. Along each of the three axes, the stage was moved in steps of 1 mm over a total distance of 60 mm.

2.2.2 | Relative 3D dose-distribution measurements in water

The dose distribution of the P50 source was determined through the percentage depth dose (PDD) and the beam profile at selected depths. These measurements were performed in two steps in the water phantom. First, the measurements were performed with the PSD and then repeated with the BF. This allowed for direct subtraction of the stem signal. Due to discrepancies in coupling efficiency between the optical fiber and PMT, the stem signal in the PSD and BF probes could differ. This was accounted for in the following way. Just before a probe was used for 3D measurements, its fiber-optic cable was stretched out on a table, with a block of solid water placed under the cable 2 m from the probe tip. This point was then irradiated for 20 seconds with P50. This provided two signals, C_{PSD} and C_{BF}, assumed to be purely from luminescence in the optical fibers. The ratio between the PSD and BF probes' stem-signal was then given as $R_{PSD/BF} = C_{PSD}/C_{BF}$. This factor was used to account for differences in coupling efficiency.

For the 3D dose measurements, the PSD probe was placed, pointing vertically upward, on the MP3s movable stage with the in-house built plastic holder. The P50 applicator was placed, pointing vertically downward, on the MP3 water phantom with the in-house build scaffold (Figure 1d–e). The applicator tip was covered with a thin rubber film to prevent water from entering. The phantom was filled with water until the P50 applicator breached the surface by approximately 1 mm. The longitudinal axis of the PSD probes was aligned with that of the P50 applicator. The probe tip was aligned with the applicator's opening plane by just letting the tip contact the rubber film. This point was defined as the origin. To measure the PDD, the P50 irradiation was turned on, and the PSD moved to source-to-detector distances (SDDs) between 0 and 48 mm in steps of 1 mm to 3 mm along the applicator's central axis. The PSD was measured for 2 seconds at each position. The beam profiles were measured by placing the PSD –40 mm off-center, turning the P50 on and stepping the PSD across the P50 center to +40 mm. The step sizes ranged from 0.5 mm to 5 mm, measuring for 2 seconds at each position. This was done along two perpendicular axes and repeated for SDDs of 5 mm, 10 mm, 20 mm, 30 mm, and 50 mm. Irradiation was turned off for 10 minutes between each SDD, and the background signal, S_{BG}, was measured for 5 min.

2.2.3 | Data analysis for the PDD

The data analysis was performed with custom-built Python scripts. The main analysis consisted of identifying and quantifying the various contributions to the relative dose from the performed measurements. The dose as measured with the PSD, D_{PSD}, at a given source-to-detector position (SDP), r, was written

$$D_{PSD}(r) = \left[L\left(\dot{S}_{PSD}(r)\right) \times S_{PSD}(r) - S_{BG1}(r) - \left(R_{\frac{PSD}{BF}} \times S_{BF}(r) - S_{BG2}\right)\right] \times E(r) \quad (1)$$

$S_{PSD}(r)$ is the signal as measured with the PSD at position r. It was composed of all possible contributions. $S_{BF}(r)$ is the corresponding measurement with the BF probe. S_{BGi} is the background signal from the PSD ($i = 1$) and bare-fiber probe ($i = 2$). All units were given as the accumulated charge during measurement at a single position, multiplied by a constant factor. The signals are therefore reported in arbitrary units. The uncertainty of D_{PSD} was determined via the law of error propagation using Equation (1). The uncertainty of the measured contributions was determined as ±1 SD. The SD of parameters derived from multiple measurements ($R_{PSD/BF}$, L, and E) were also determined with the law of error propagation.

2.2.4 | 3D dose measurement validation with Monte Carlo

The 3D dose measurements were validated against a corresponding MC simulation. For this simulation, the accelerated electrons, bremsstrahlung, and filtering processes in P50 were all included to gain the correct shape and angular distribution of the photon beam. Physical and material properties were defined as in the subsection "PSD energy dependence", if not stated otherwise. The simulation was divided into two parts. One is the generation of the source photons via simulation of the bremsstrahlung process. This simulation is very time consuming, and the photons were therefore *recorded* in phase space files (PSFs). This allowed for later replay of the photon tracks skipping the bremsstrahlung process. Two: The PSFs were displayed into a water phantom to score the 3D dose distribution.

For part one, the X-ray tube geometry was built according to the literature.[5,27] All materials were taken from the Geant4 materials list.[29] The source was defined as a 2 mm diameter disc, emitting electrons with a uniform distribution toward a rhenium target. The electron energy spectrum was defined as a Gaussian distribution around 47.6 keV to match the maximum value of the measured P50 spectrum (more detail is provided in Section 3.1 and Figure 4) with a full width at half maximum (FWHM) of 5%. Croce et al. reported a maximum energy of 48.5 keV.[5] Simulations with an electron energy spectrum around this value were also performed to investigate the effect of the variations in the P50 potential.

An uncertainty related to the P50 potential was determined as one half of the deviation in the depth dose curves calculated using 47.6 and 48.5 kV, respectively (Figure S1).

Some variance reduction techniques were implemented to shorten the simulation time. For the bremsstrahlung interaction, a directional filter was defined so that only secondary photons with direction toward the beryllium filter were simulated. These photons were also subjected to splitting. The energy and direction of photons passing through the beryllium filter were recorded in 23 PSFs. This simulation secured the correct shape and angular distribution of the photon beam.

For part two, the P50 applicator and a cubic water phantom of 600 × 600 × 600 mm^3 were implemented, with the applicator opening in the plane of the water surface. The beryllium filter was defined as the photon source, and 23 PSFs were used to generate particle tracks. The dose distribution was scored in the water phantom in 1 mm^3 voxels of water. For this part, no variance reduction techniques were used. The PSF files did not contain enough photon histories to make the dose distribution converge. Therefore, each PSF was reused 500 times, but each time the source randomly rotated along the applicator's central axis and a new starting seed. The statistical uncertainty of the scored dose was determined as the estimated SD of the scored dose per 10 000 PSF runs (Figure S2).

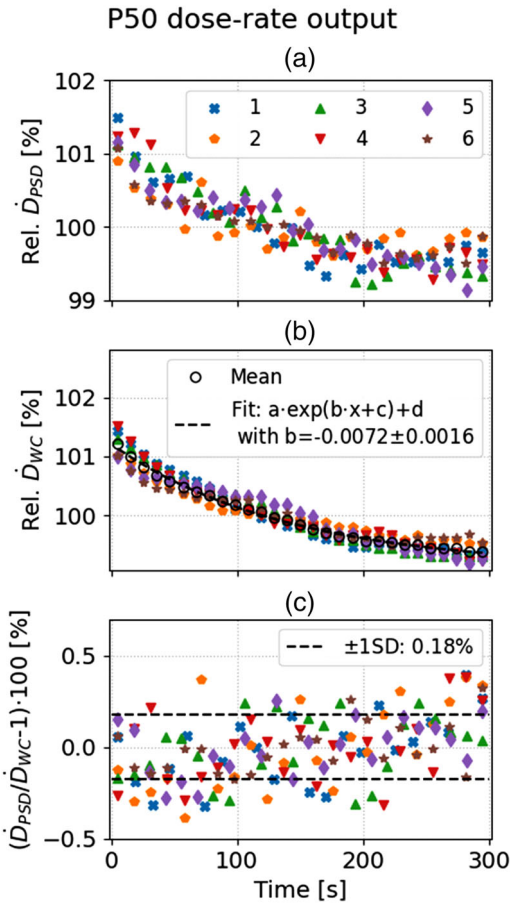

FIGURE 2 The relative output dose rate of the P50 as measured with (a) the PSD and (b) with the WTCh during 6 irradiations. Each of the six measurements is plotted with distinct symbols. All measurements are normalized to the mean value (the dashed line is an exponential fit to the mean of the six normalized measurements). (c) The deviation between the normalized WTCh and PSD measurements

3 | RESULTS

3.1 | Detector stability, dose-rate-response, and energy dependence

An exponential decrease over time in the signal was measured by both detectors (Figure 2a–b). This was assumed to stem from a decrease in the output dose rate of the P50. An exponential fit was made to the WTCh signal (Figure 2b) and used in the PDD and dose profile analysis to account for output dose-rate changes over time. The PSD showed larger fluctuations in the signal than the WTCh, but they were always within 0.4% of each other with an SD of 0.18% when both signals were normalized to their mean over the entire irradiation period (Figure 2c).

The relative response of the PSD decreases linearly by 0.38% for every 1000 au increase in $\dot{S}_{PSD}$ (Figure 3a). The linearity factor is then given by the inverse of this relation:

$$L\left(\dot{S}_{PSD}\right) = \left[\left(-3.7766 \times 10^{-6} \pm 5 \times 10^{-7}\right) \times \dot{S}_{PSD} + 1.015786 \pm 2 \times 10^{-6}\right]^{-1}. \quad (2)$$

The MC simulation showed that more dose is deposited in water compared to polystyrene, close to the source (Figure 3b). The ratio between the relative dose to water and polystyrene then drops by 0.84% per 10 mm depth. The energy-correction factor is defined as a linear fit to this ratio vs. depth (in mm)

$$E\ (r) = \left(-8.4 \times 10^{-3} \pm 3 \times 10^{-5}\right) \times r + 1.0146 \pm 3 \times 10^{-4}. \quad (3)$$

The measured spectra used for determining the energy dependence and the scored spectra resulting from simulating the entire P50 source showed some discrepancies (Figure 4). A peak was observed around 23 keV for the measurements not observed in the simulation, and the simulated spectrum seemed slightly hardened and skewed to the right compared to the measured spectrum.

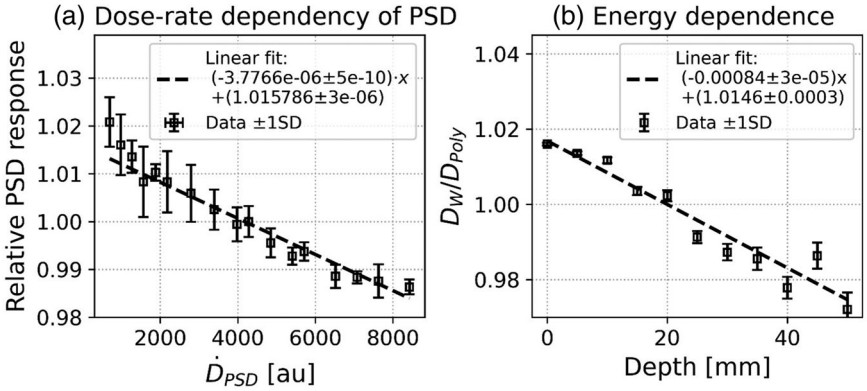

FIGURE 3 a) The relative response of the PSD as a function of dose rate (squares). Error bars indicate ±1 SD. The data are normalized to the measurements taken at a tube current of 1.5 mA in P50. b) The ratio of Monte Carlo scored dose to water and polystyrene as a function of depth in water when exposed to the P50 spectrum (squares). Data are normalized to a depth of 20 mm. Error bars indicate ±1 SD. In both figures, the dashed line is a linear fit to the measurements.

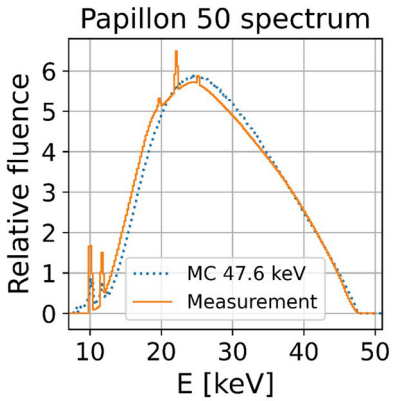

FIGURE 4 The spectrum of a P50 eBT source as measured in air at a 25 cm distance (solid line) and gained from Monte Carlo simulation (dotted line)

3.2 | Precision of MP3 phantom stage positioning

The SDs between the video tracked and expected positions of the phantom ranged from 0.08 to 0.1 mm (Figure 5). Assuming this uncertainty holds for the initial positioning of the dosimeter, a conservative estimate of the total positional uncertainty of the dosimeter is then 0.2 mm by adding the uncertainties in quadrature (0.1 mm between positions and 0.1 mm for each axis at initial positioning).

3.3 | Relative 3D dose distribution in water

The PDD curves showed a greater than 10-fold reduction at 30 mm depth relative to 0 mm depth (Figure 6a). The measured PDD curve took approximately 200 s to measure, both for the PSD and BF probes. Taking all terms in Equation 1 into account, D_{PSD} and D_{MC} agreed within 2% except for 0 mm depth and at 43 mm depth (Figure 6b). The stem effect contributed to 1% of the total signal closest to the source and increased gradually to 3% farthest from the source.

The beam profiles at each depth and axis took 350 s to measure for both the PSD and BF probes. The beam profiles showed a width of 25.5(5) mm on the end of the 25 mm applicator (Figure 7) when extrapolating the FWHM of the profiles back to 0 mm depth. The beam profile broadens and flattens with 0.66(2) mm per mm SDD (Figure 7f). This is slightly less than the 0.74(1) mm per mm SDD determined through MC simulations. The dose gradient is very steep at the profile edges, ranging from 15%/mm at 50 mm SDD to 50%/mm at 5 mm SDD. The measured profiles along the *x*- and *y*-axes are similar, and both exhibit a shoulder to the right. At 5 mm depth, this causes a 15% difference in dose between the right- and left-hand side 10 mm away from the central axis. The difference is reduced with increasing depth. At the central plateau, the stem-effect contribution corresponded to the PDD measurements. The stem effect was largest at distances of 20–40 mm from the center. Here, it constituted up to 18% of the total signal at 5 mm depth and gradually dropped to 6% at 50 mm depth. At 45 mm from the center, the stem effect was undetectable at all depths.

3.4 | Uncertainty contributions

Table 1 shows the uncertainty of the contributions to the relative dose as measured with the PSD in terms of Equation 1. The uncertainties are position dependent and therefore the largest uncertainties are reported. The largest uncertainties stem from the intrinsic uncertainty of the detector (up to 1.3%) and the linearity factor (up to 1.7%).

4 | DISCUSSION

This work presents the performance of a PSD system for the relative dosimetry of very low-energy X-rays in water. The PDD of a P50 source was measured with 2.5% uncertainty in the range of 0 to 50 mm SDD and a positional uncertainty of 0.4 mm. Thus, even at distances above 40 mm away from the source, the PSD

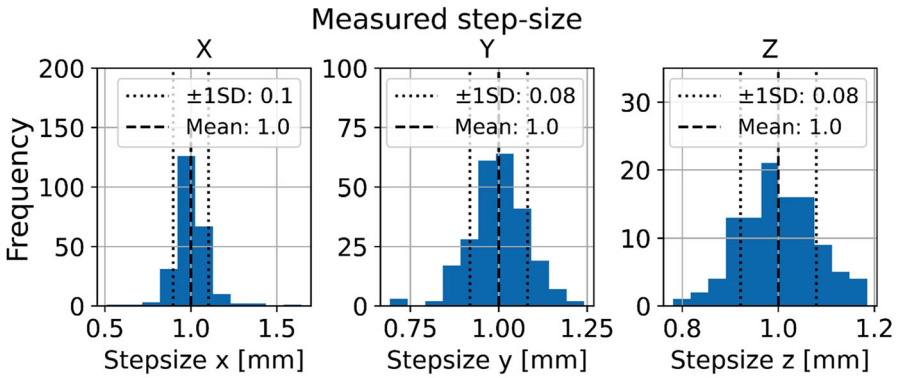

FIGURE 5 Histogram of the measured phantom stage step-size when expecting 1 mm steps along the three axes of movement. The SD along each axis is denoted with dotted lines, and the mean step size is denoted with dashed lines

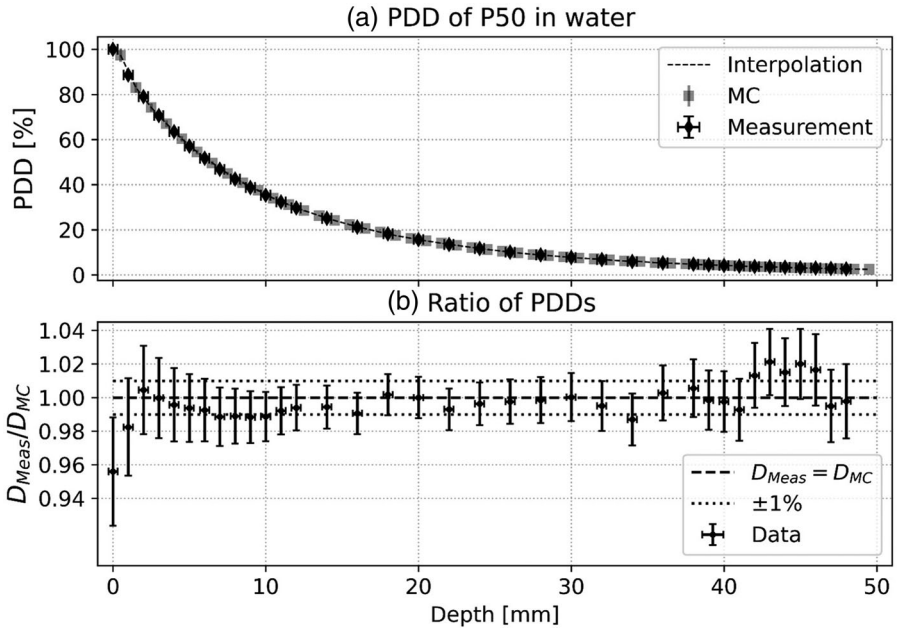

FIGURE 6 (a) PDD curve as measured with the PSD (diamonds) and scored with Monte Carlo simulation (squares). The dashed line is a linear interpolation of the MC results. Error bars indicate ±1 SD. (b) The ratio between the measured and scored doses (dots). Error bars indicate ±1 SD. Lines denote 0% (dashed) and 1% (dotted) deviations

provided a relative dose measurement within the recommendation limits of the AAPM (5%). The dose profiles provide useful insight into the field shape and the dose distribution of the P50. This was seen from the clear dose difference at equidistant opposite positions around the applicator's central axis. This shape variability is likely specific for individual P50 units, and therefore the data provided in this study should not act as a clinical reference. However, the described method provides a reliable validation of the dose distribution if used for any P50 unit. While a long time was dedicated to establishing a suitable method for the actual dose measurements, the measurements themselves were performed within 8 h. Approximately 1 h for preparing the setup, ~2 h of dose measurements, and ~4 h total break between irradiations to cool down the P50 and switch between PSD and BF probe. Annual dose verification, for which detector dose-linearity and stability verification might not be necessary, is therefore realistic with the presented setup. The BF measurements are necessary, as the stem effect contributed substantially to the total signal. Ideally, the outermost 0.5 mm of the BF should consist of polystyrene, rather than PMMA, since different plastics will exhibit different fluorescence properties. However, due to the small size of the scintillating fiber, the main stem contribution originates from the PMMA fiber. Therefore, the small discrepancy in the stem signal due to different plastics in the probe tips was deemed negligible. Previously, a full dose distribution measurement of the P50 was only performed in plastic phantoms,

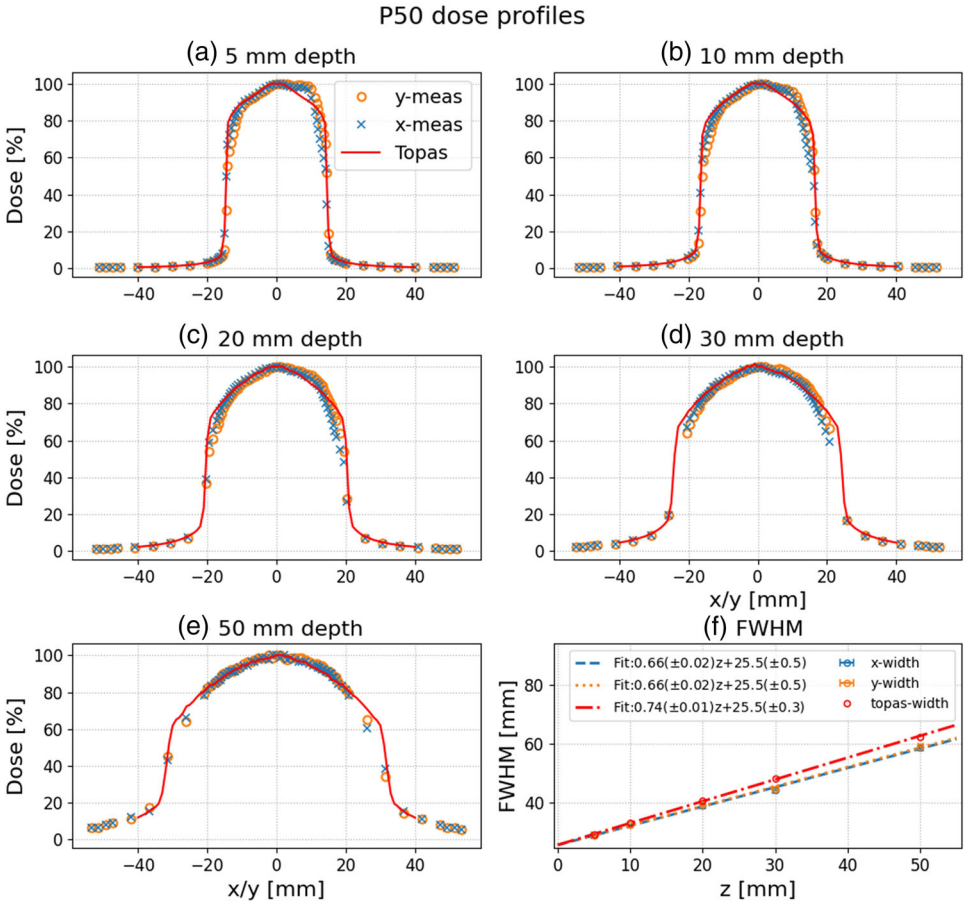

FIGURE 7 Dose profiles as measured along the x-axis (crosses) and y-axis (circles) and scored with MC simulation (solid line). Figure f) shows the FWHM of the profiles (dots) as a function of depth along with linear fits (dashed line along x-axis measurements, dotted line along *y*-axis measurements, and dotted-dashed line for MC results)

with the most prominent example being Croce et al.'s work in 2012.[5] Their results showed the importance of dosimetry in water since simulation of the PDD showed a clear discrepancy between dose to water and dose to PMMA. One should also note that their simulation defined the P50 as a 48.6 kVp source as opposed to the 47.6 kVp used in this study. In this study, this value was based on a measurement of the P50 spectrum. Discrepancy from the nominal 50 kVp potential changes beam quality and thereby dose distribution. The PRISM-eBT collaboration[24] has assembled a catalog in which nominal spectra from a range of eBT sources are provided. While the dose distribution changes with small spectrum changes, the energy correction factor of the PSD, being nearly linear with depth, is likely robust toward small tube potential changes. Thus, these spectra will likely be sufficient for acceptable energy correction calculations, although proper MC calculations of dose distribution should be performed with the actual tube potential. Further investigation should also include a characterization of the discrepancies in measured and simulated spectra (Figure 4). The peak observed at approximately 22 keV for the measurement is suspected to stem from silver being present in the beam filter, despite not being presented in the literature on which the simulation was based.[5,27] Additionally, the MC spectrum was hardened compared to measurements, suggesting additional filtering. This could be caused by heterogeneities in the construction of the beam filter, which will be addressed later. The stability of the P50 potential should also be investigated. The 1 keV discrepancy in maximum spectrum energy between this study and the one of Croce et al indicates large variation in the P50 potential. The two spectra are measured with two different P50 values, which most likely will lead to a larger fluctuation than that observed over time within a single P50. The estimated uncertainty for the Monte Carlo simulation is therefore also likely overestimated, Table 1. The robustness of this study's correction factors toward these effects should be investigated.

Although this experiment was specifically designed for the P50 source, the method could be expanded to other eBT sources with appropriate modifications. The INTRABEAM (Carl Zeiss Surgical, Germany) and Xoft

TABLE 1 Estimated uncertainty contribution to the relative dose as measured with the PSD and scored with MC from each component

Term	Description	Relative uncertainty contribution, σ (%)
	Measurement uncertainties	
S_{PSD}	The raw signal from the PSD, for which the uncertainty is determined from the stability measurements	1.3
L	Dose-rate response linearity factor	1.7
$R_{PSD/BF}$	Normalization factor for stem-effect in PSD and BF probe	0.4
S_{BF}	The raw signal from the BF probe, from which the uncertainty is determined from the above factor	0.4
S_{BG1}	The background signal when measuring with PSD. Undetectable in current setup, and therefore set to the minimally detectable value	0.5
S_{BG2}	The background signal when measuring with the BF probe. Undetectable in current setup, and therefore set to the minimally detectable value	0.5
E	The energy-correction factor	0.8
r	The relative position between the source and detector	$\pm$ 0.2 mm
$\boldsymbol{D_{PSD}}$	**The reported relative dose, $(\sum\sigma^2)^{1/2}$**	**2.5**
	Monte Carlo simulation uncertainties	
D_{stat}	The statistical uncertainty based on the number of simulations performed, see also figure 1S in the supplementary material	1.2
$Dspec$	The uncertainty stemming from uncertainty in the P50 potential and hence the energy spectrum, Figure 4	3.5
$\boldsymbol{D_{MC}}$	**The reported relative dose, $(\sum\sigma^2)^{1/2}$**	**3.7**

Axxent (iCAD Inc., US) eBT sources work more similarly to conventional radioisotope BT. Dosimetry for these devices has been performed in terms of radial dose and an-isotropy functions. The radial dose was determined with miniature parallel-plate ionization chambers, and an-isotropy was analyzed with radio chromic films.[7,30–33] Holders could be manufactured for these eBT sources, and the PSD system could be used to provide both radial dose and an-isotropy measurements. The estimated uncertainty of the PSD system is equal to or lower than the reported uncertainties for dosimeters used for INTRABEAM dosimetry,[9] although for a fair and direct comparison, a calibration procedure for absolute dose measurements with the PSD must be considered along with differences in the P50 and INTRABEAM geometry and beam quality.

Until now, the PSD has not been thoroughly characterized for X-rays below 50 keV. Therefore, the factors contributing to the uncertainty of the PSD signal were investigated and quantified to determine its reliability and feasibility. The stability and dose–response linearity of the PSD signal were investigated by comparing it to the signal of a WTCh under identical irradiation conditions. The PSD signal fluctuated with a standard deviation of 0.1% at the highest dose rates to 1.3% at the lowest, and the system's intrinsic uncertainty was therefore relatively small. The response efficiency of the PSD decreased linearly with dose rate, and correcting for this nonlinearity of the dose-rate response constituted the largest uncertainty of the total signal. The given linearity factor is likely to be of acceptable for many irradiations since PSDs have been shown to be robust toward scintillation deterioration. They experience only a small gradual decrease in light emission with accumulated dose.[20,34] Studies have shown that the relative response and quenching of plastic scintillators at these energies change substantially with small changes in photon energy[20–23], and the intrinsic scintillation response of a specific PSD must therefore be comprehensively known. Therefore, this investigation used MC to score the relative dose to water and polystyrene to correct for the energy-dependent response of the scintillator, and the intrinsic energy dependence of the PSD was thus not investigated. This method was deemed appropriate since studies have shown that the relative response of polystyrene-based scintillators is nearly identical across different dissolved active fluors

(BCF-10, BCF-12, BCF-60) below 100 keV.[21–23] The same studies showed that quenching, despite being considerable at low photon energies, stays nearly constant in radiation geometries and energies such as those investigated here. Therefore, quenching was not considered in this study. The good agreement between the measured and scored doses to water was an indication that this approach was feasible. Investigation of the relative scintillator response to mono-energetic beams or investigation of more PSDs is still warranted for full validation.

The steep dose gradient associated with low-energy X-rays demands a high accuracy of SDD. The results in Figure 3 show that the phantom stage could be moved to desired positions with a precision of < 0.1 mm for small movement steps, in exact agreement with the manufacturer's stated uncertainty (see note 1). The initial placement of the detector probe and source is therefore the largest contributor to positional uncertainty, adding at most 0.3 mm. In a clinical context, where applicators are placed by hand, often purely based on visual inspection of the tumor, this uncertainty must be considered satisfactorily small for dose-distribution verification.[1,3]

The simulated and measured widths of the dose profiles did not agree. This might be due to a small positional shift between the X-ray tube and applicator. If the X-ray tube tip and applicator opening are further apart than assumed, the exit angle of the beam would decrease, causing the profile widths to increase at a slower rate, as observed (Figure 7f). This shift could be simulated in further investigations. The measured profiles also showed asymmetry not seen in the MC results, where perfect symmetry was assumed. This indicates the need for experimental validation. The asymmetry is likely due to unintended heterogeneities in the construction of or damage to the beam filter in the used P50. An important finding, given that a highlighted selling point for the Papillon systems are their highly symmetric dose profiles. Based on their own profile measurements, Croce et al. recommended that the manufacturer should provide new filters to end users to improve beam shape.[5] The P50 used in this study has not been changed since it was acquired and thus should be subject to the same potentially flawed filtering. Ariane provides services for periodic check of the beam flatness, but the tolerance is quite high ($< 5\%$ variation within the central 80% of the beam width)[2]. The method provided in this paper lays forth an independent way to verify these checks and provide additional information on the dose distribution. It should be noted that an energy-dependence correction factor was not applied to the profile measurements. Due to the P50s geometry and the initial direction of X-rays, the spectrum is expected to be close to identical along the profile at a given depth, with a possible exception at the profile edges. However, due to the extremely steep dose gradients at the edges, the FWHM should be representative of the actual confinement of the dose distribution in water.

[2] Mail correspondence with Ariane Medical Systems.

5 | CONCLUSION

The combination of a PSD and a motorized water phantom proved to be a feasible setup for measuring the relative dose distribution in water of the P50 eBT source with < 0.4 mm positional uncertainty. The PDD curve was measured with an uncertainty of $< 2.5\%$. Additionally, dose profiles were measured at 5 different depths, effectively providing the full 3D dose distribution. The method is suitable for at least annual dose-distribution verification of eBT sources. Thirty-four of 36 PDD points agreed within 2% of the MC results. MC simulations are planned to be verified further in future investigations, solidifying its use as a validation tool for eBT dosimetry. Although the experiment was designed for the P50 eBT unit, many eBT sources work similarly, and the method can thus likely be transferred to other sources.

ACKNOWLEDGEMENTS

This study has received funding from the EMPIR programme (grant 18NRM02 PRISM-eBT) co-financed by the Participating States and from the European Union's Horizon 2020 research and innovation Programme and from Novo Nordisk Fonden (grant NNF19OC0058756).

CONFLICTS OF INTEREST

The authors have no conflicts of interest to disclose.

DATA AVAILABILITY STATEMENT

The authors will share data upon request to the corresponding author.

REFERENCES

1. Hensley FW. Present state and issues in IORT physics. *Radiat Oncol*. 2017; 12(1): 37. https://doi.org/10.1186/s13014-016-0754-z.
2. Ma CM, Coffey CW, DeWerd LA, et al. AAPM protocol for 40–300 kV X-ray beam dosimetry in radiotherapy and radiobiology. *Med Phys*. 2001; 28(6): 868–893. https://doi.org/10.1118/1.1374247.
3. Eaton DJ. Electronic brachytherapy—current status and future directions. *Br J Radiol*. 2015; 88(1049): 20150002. https://doi.org/10.1259/bjr.20150002.
4. Brahme A. Dosimetric precision requirements in radiation therapy. *Acta Radiol Oncol*. 1984; 23(5): 379–391. https://doi.org/10.3109/02841868409136037.
5. Croce O, Hachem S, Franchisseur E, Marcié S, Gérard JP, Bordy JM. Contact radiotherapy using a 50 kV X-ray system: evaluation of relative dose distribution with the Monte Carlo code PENELOPE and comparison with measurements. *Radiat Phys Chem*. 2012; 81(6): 609–617. https://doi.org/10.1016/j.radphyschem.2012.01.033.
6. Hill R, Mo Z, Haque M, Baldock C. An evaluation of ionization chambers for the relative dosimetry of kilovoltage X-ray beams. *Med Phys*. 2009; 36(9 Part1): 3971–3981. https://doi.org/10.1118/1.3183820.

7. Watson PGF, Bekerat H, Papaconstadopoulos P, Davis S, Seuntjens J. An investigation into the INTRABEAM miniature X-ray source dosimetry using ionization chamber and radiochromic film measurements. *Med Phys*. 2018; 45(9): 4274–4286. https://doi.org/10.1002/mp.13059.
8. Watson PGF, Popovic M, Seuntjens J. Determination of absorbed dose to water from a miniature kilovoltage X-ray source using a parallel-plate ionization chamber. *Phys Med Biol*. 2017; 63(1): 015016. https://doi.org/10.1088/1361-6560/aa9560.
9. Eaton DJ. Quality assurance and independent dosimetry for an intraoperative X-ray device. *Med Phys*. 2012; 39(11): 6908–6920. https://doi.org/10.1118/1.4761865.
10. Hoerner MR, Stepusin EJ, Hyer DE, Hintenlang DE. Characterizing energy dependence and count rate performance of a dual scintillator fiber-optic detector for computed tomography. *Med Phys*. 2015; 42(3): 1268–1279. https://doi.org/10.1118/1.4906206.
11. Hyer DE, Fisher RF, Hintenlang DE. Characterization of a water-equivalent fiber-optic coupled dosimeter for use in diagnostic radiology. *Med Phys*. 2009; 36(5): 1711–1716. https://doi.org/10.1118/1.3116362.
12. Beddar AS, Mackie TR, Attix FH. Water-equivalent plastic scintillation detectors for high-energy beam dosimetry: iI. Properties and measurements. *Phys Med Biol*. 1992; 37(10): 1901–1913. https://doi.org/10.1088/0031-9155/37/10/007.
13. Therriault-Proulx F, Beaulieu L, Archambault L, Beddar S. On the nature of the light produced within PMMA optical light guides in scintillation fiber-optic dosimetry. *Phys Med Biol*. 2013; 58(7): 2073–2084. https://doi.org/10.1088/0031-9155/58/7/2073.
14. Frelin AM, Fontbonne JM, Ban G, et al. Spectral discrimination of Čerenkov radiation in scintillating dosimeters. *Med Phys*. 2005; 32(9): 3000–3006. https://doi.org/10.1118/1.2008487.
15. Kertzscher G, Beddar S. Inorganic scintillation detectors for 192Ir brachytherapy. *Phys Med Biol*. 2019; 64(22): 225018. https://doi.org/10.1088/1361-6560/ab421f.
16. Archambault L, Therriault-Proulx F, Beddar S, Beaulieu L. A mathematical formalism for hyperspectral, multipoint plastic scintillation detectors. *Phys Med Biol*. 2012; 57(21): 7133–7145. https://doi.org/10.1088/0031-9155/57/21/7133.
17. Therriault-Proulx F, Archambault L, Beaulieu L, Beddar S. Development of a novel multi-point plastic scintillation detector with a single optical transmission line for radiation dose measurement. *Phys Med Biol*. 2012; 57(21): 7147–7159. https://doi.org/10.1088/0031-9155/57/21/7147.
18. Darafsheh A, Zhang R, Kanick SC, Pogue BW, Finlay JC. Spectroscopic separation of Čerenkov radiation in high-resolution radiation fiber dosimeters. *J Biomed Opt*. 2015; 20(9): 095001. https://doi.org/10.1117/1.JBO.20.9.095001.
19. Darafsheh A, Melzer JE, Harrington JA, Kassaee A, Finlay JC. Radiotherapy fiber dosimeter probes based on silver-only coated hollow glass waveguides. *J Biomed Opt*. 2018; 23(1): 015006. https://doi.org/10.1117/1.JBO.23.1.015006.
20. Beddar AS, Mackie TR, Attix FH. Water-equivalent plastic scintillation detectors for high-energy beam dosimetry: i. Physical characteristics and theoretical considerations. *Phys Med Biol*. 1992; 37(10): 1883–1900. https://doi.org/10.1088/0031-9155/37/10/006.
21. Boivin J, Beddar S, Bonde C, et al. A systematic characterization of the low-energy photon response of plastic scintillation detectors. *Phys Med Biol*. 2016; 61(15): 5569–5586. https://doi.org/10.1088/0031-9155/61/15/5569.
22. Ebenau M, Radeck D, Bambynek M, et al. Energy dependent response of plastic scintillation detectors to photon radiation of low to medium energy. *Med Phys*. 2016; 43(8 Part1): 4598–4606. https://doi.org/10.1118/1.4957348.
23. Lessard F, Archambault L, Plamondon M, et al. Validating plastic scintillation detectors for photon dosimetry in the radiologic energy range. *Med Phys*. 2012; 39(9): 5308–5316. https://doi.org/10.1118/1.4738964.
24. Primary standards and traceable measurement methods for X-ray emitting electronic brachytherapy devices. Accessed October 29, 2021. http://www.ebt-empir.eu/wp-content/uploads/Publishable-Summary-M18.pdf
25. Perl J, Shin J, Schümann J, Faddegon B, Paganetti H. TOPAS: an innovative proton Monte Carlo platform for research and clinical applications. *Med Phys*. 2012; 39(11): 6818–6837. https://doi.org/10.1118/1.4758060.
26. Faddegon B, Ramos-Méndez J, Schuemann J, et al. The TOPAS tool for particle simulation, a Monte Carlo simulation tool for physics, biology and clinical research. *Phys Med*. 2020; 72: 114–121. https://doi.org/10.1016/j.ejmp.2020.03.019.
27. Gérard JP, Myint AS, Croce O, et al. Renaissance of contact X-ray therapy for treating rectal cancer. *Expert Rev Med Devices*. 2011; 8(4): 483–492. https://doi.org/10.1586/erd.11.28.
28. Low energy electromagnetic physics - Penelope | geant4.web.cern.ch. Accessed October 29, 2021. https://geant4.web.cern.ch/node/1621
29. Geant4 material database — book for application developers 10.7 documentation. Accessed October 29, 2021. https://geant4-userdoc.web.cern.ch/UsersGuides/ForApplicationDeveloper/html/Appendix/materialNames.html
30. Ebert MA, Carruthers B, Lanzon PJ, et al. Dosimetry of a low-kV intra-operative X-ray source using basic analytical beam models. *Australas Phys Eng Sci Med*. 2002; 25(3): 119–123. https://doi.org/10.1007/BF03178772.
31. Beatty J, Biggs PJ, Gall K, et al. A new miniature X-ray device for interstitial radiosurgery: dosimetry. *Med Phys*. 1996; 23(1): 53–62. https://doi.org/10.1118/1.597791.
32. Eaton DJ, Duck S. Dosimetry measurements with an intra-operative X-ray device. *Phys Med Biol*. 2010; 55(12): N359–N369. https://doi.org/10.1088/0031-9155/55/12/N02.
33. Rivard MJ, Davis SD, DeWerd LA, Rusch TW, Axelrod S. Calculated and measured brachytherapy dosimetry parameters in water for the Xoft Axxent X-ray source: an electronic brachytherapy sourcea). *Med Phys*. 2006; 33(11): 4020–4032. https://doi.org/10.1118/1.2357021.
34. Li Z, Chong W, Yuekun H, et al. Properties of plastic scintillators after irradiation. *Nucl Instrum Methods Phys Res Sect Accel Spectrometers Detect Assoc Equip*. 2005; 552(3): 449–455. https://doi.org/10.1016/j.nima.2005.06.075.

SUPPORTING INFORMATION

Additional supporting information may be found in the online version of the article at the publisher's website.

How to cite this article: Georgi P, Kertzscher G, Nyvang L, et al. Toward 3D dose verification of an electronic brachytherapy source with a plastic scintillation detector. *Med Phys*. 2022;49:3432–3443. https://doi.org/10.1002/mp.15568